

Universitat de Lleida

Economic Viability

Made by
Oriol Alàs Cercós

Delivery
25th of May, 2022

Universitat de Lleida
Escola Politècnica Superior
Màster en Enginyeria Informàtica
Technological Business Management and Entrepreneurship

Professorate:

Josep Escribà Garriga

Contents

1	Introduction	1
2	Problem Analysis	2
2.1	Sentinel2	2
2.2	Related work and state-of-the-art	4
2.3	Academic Datasets	17
3	Model architecture	17
4	Experiments & results	17
5	Conclusions	17
6	Bibliography	17

List of Figures

1	LeNet-5 architecture.	4
2	Residual learning: a building block.	5
3	DSen2-CR model diagram.	5
4	Examples of the influence of SAR data. Being (a, f) cloudy images, (b, g), SAR images, (c, h), the target cloudless images, (d, i), the synthesized images without SAR input data and (e, j) the predictions using SAR data as input.	6
5	GAN model diagram.	7
6	cGAN model diagram.	8
7	Prediction results by McGAN with the synthesized cloud images	9
8	Prediction results by McGAN with the real cloud images	10
9	Comparison between the cloudy images, the outputs of McGAN and Pix2Pix-based models and the ground-truth image.	11
10	Comparison between cloudy images, the outputs of McGAN versions and the ground-truth image.	12
11	Failure cases in CloudGAN attempting to removal overly clouded images over-smoothening or completely failing.	14

12	Failure cases in CloudGAN attempting to removal overly clouded images over-smoothening or completely failing.	15
13	Transformer block architecture. left block , the encoder architecture, right block , the decoder architecture.	15

List of Tables

1	Sentinel 2 bands	2
2	PSNR and SSIM of the single-image and multi-temporal model versions . .	12

Acronyms

cGAN Conditional Generative Adversarial Network.

CNN Convolutional Neural Network.

GAN Generative Adversarial Network.

IR Infra Red.

L1C Level-1C.

L2A Level-2A.

McGAN Multi-spectral Conditional Generative Adversarial Network.

MLP Multi-Layer Perceptron.

NIR Near Infra Red.

NLP Natural Language Processing.

PSNR Peak signal-to-noise ratio.

RS Remote Sensing.

SAR Synthetic Aperture Radar.

SSIM Structural Similarity Index Metric.

1 Introduction

Remote Sensing (RS) imagery is critical to perform challenges such climate change or natural resources management, including zone monitoring for reforestation, disaster mapping, land surface change detection and coastal water quality monitoring. Nevertheless, on average 55% of the Earth's land surfaces is covered by clouds, being then a significant impediment to carry out a broad range of applications. Satellite imagery plagued by films of clouds that obstructs the scene implies a great loss of information or causing effects such as blurring, which mitigates the power of RS. Hence, RS applications definitely needs a generic technique to detect and remove the cloudy region with an in-painting of the underlying scene.

Once set the problem, the goals of this master thesis have been:

- Search state-of-the-art solutions as well as technologies that could bring new improvements and better results.
- Create or search for a multi-temporal and spatial imagery to design and evaluate general solutions.
- Design and implement an effective model and monitoring its training.
- Evaluate the model and make a comparison with the other solutions proposed.

2 Problem Analysis

2.1 Sentinel2

The analysis of the problem has been focused using Copernicus Sentinel2 constellation. Sentinel2 images are provided by two satellites, Sentinel 2A and Sentinel 2B, which orbit each other with a 180° phase shift. Generally, the acquisition of the images is more or less 10 days per satellite so that a new updated image of a specific area is available in periods of time not exceeding five days. This makes Sentinel-2 data an excellent choice for studying environmental challenges. Sentinel-2 products are a compilation of elementary granules of fixed size, within a single orbit. A granule, also called tile, is a multi-spectral image with 13 bands in the visible, near-infrared, and short-wave infrared spectrum. These bands come in a different spatial resolution ranging from 10m to 60m, so the images can be classified as medium-high resolution. All the granules are 100x100km² ortho-images in UTM/WGS84 projection. There are five types of Sentinel-2 data although only two are available for users: Level-1C (L1C) and Level-2A (L2A). The difference between them is that the latter provides background reflectance imagery of the atmosphere derived from associated L1C products. In 1, there are the bands with its most high resolution and ordered by its central wavelength, being B5-B12 Near Infra Red (NIR) or Infra Red (IR) bands.

Table 1: Sentinel 2 bands

Band	Name	Central wavelength (μm)	Bandwidth (nm)	Spatial resolution (m)
B1	Coastal aerosol	0.433	27	60
B2	Blue	0.490	98	10
B3	Green	0.560	45	10
B4	Red	0.665	38	10
B5	Vegetation Red Edge	0.705	19	20
B6	Vegetation Red Edge	0.740	18	20
B7	Vegetation Red Edge	0.783	28	20
B8	NIR	0.842	125	10
B8A	Vegetation Red Edge	0.865	33	20
B9	Water Vapour	0.945	26	60
B10	SWIR-Cirrus	1.375	75	60
B11	SWIR	1.610	143	20
B12	SWIR	2.190	242	20

The bands can give us a various range of aspects of the orthogonal view. Several spectral indices have been created over the years by performing operations between the

bands, which can broaden the range of analysis and make them more accurate to finally better understand the features in the imagery. The most used bands to generate indices are B3, B4 and B8. The following list explains some of the most popular:

NDVI The Normalized Difference Vegetation Index is highly associated with the vegetation content. Higher values of NDVI correspond to areas that reflect more in the near-infrared spectrum and to denser and healthier vegetation.

$$\text{NDVI} = \frac{B8 - B4}{B8 + B4}$$

GNDVI Green Normalized Difference Vegetation Index is modified version NDVI to be more sensitive to the variation of chlorophyll content in the crop.

$$\text{GNDVI} = \frac{B8 - B3}{B8 + B3}$$

NDMI Normalized Difference Moisture Index is used to determine vegetation water content.

$$\text{NDMI} = \frac{B8 - B11}{B8 + B11}$$

MSI Moisture Stress Index increases in leaf water content, so that makes it perfect for finding water stress in plants.

$$\text{MSI} = \frac{B11}{B8}$$

NBRI Normalized Burned Ratio Index detects burned areas and it is used to monitor the recovery of the ecosystem.

$$\text{NBRI} = \frac{B8 - B12}{B8 - B12}$$

BSI Bare Soil Index quantifies the soil mineral composition and the presence of vegetation.

$$\text{BSI} = \frac{(B11 + B4) - (B8 + B2)}{(B11 + B4) + (B8 + B2)}$$

NDWI Normalized Difference Water Index is used for the identification of water bodies although is sensitive to build-up land and result in over-estimated water bodies.

$$\text{NDWI} = \frac{B3 - B8}{B3 + B8}$$

NDSI Normalized Difference Snow Index identifies snow cover over land areas since in B11 snow absorbs most of the incident radiation while the clouds do not.

$$NDSI = \frac{B3 - B11}{B3 + B11}$$

2.2 Related work and state-of-the-art

Deep learning have been a popular and efficient technique to solve challenges from satellite imagery. Specifically, Convolutional Neural Network (CNN) have been the main architecture of neural networks to provide a solution from image-based problems. What differentiates CNN from the standard Multi-Layer Perceptron (MLP) is that they have hidden layers called convolutional layers, which are able to take patterns from their inputs using filters. A filter can be considered a relatively small matrix that slides from the input by operating with the weights of the matrix. This action is called *convolving* and, in its simplest case, the output value of a layer with (N, C_{in}, H, W) as the input and $(N, C_{out}, H_{out}, W_{out})$ as the output is described as:

$$out(N_i, C_{out_j}) = bias(C_{out_j}) + \sum_{k=0}^{C_{in}-1} weight(C_{out_j}, k) \star input(N_i, k)$$

where \star is the 2D cross-correlation operator, N is the batch size, C denotes the number of channels and H and W are the height and width in pixels of the planes respectively. A graphic representation of a CNN architecture can be seen in 1

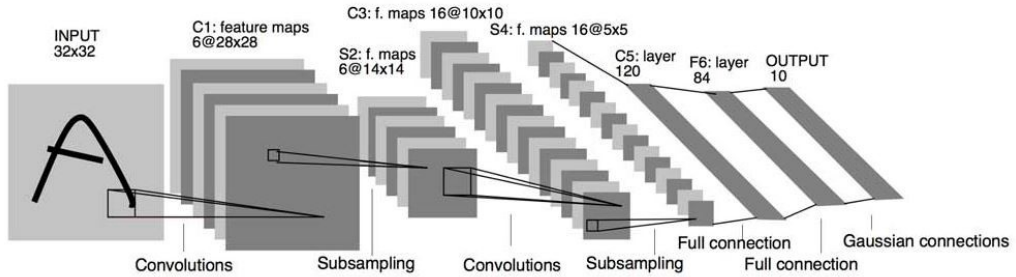


Figure 1: LeNet-5 architecture.

Being that told so, there are a lot of state-of-the-art using CNN. In [1], they create a deep learning approach to Sentinel-2 super-resolution. Their hypothesis was the existence of a complex mixture of correlations across many spectral bands over a large spatial context. Hence, the input of the model is a concatenation of the high-level resolution bands with

the low-level resolution bandwidths upsampled to 10m by simple bi-linear interpolations. The model itself is a clear reference of residual networks [2]. Furthermore, as in ResNet architectures, it uses skip connections to reduce the average effective path length through the network, alleviate the vanishing gradient problem and greatly accelerates the learning during the training.

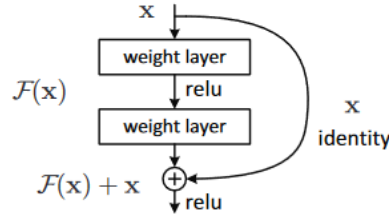


Figure 2: Residual learning: a building block.

Similarly, in [3], a residual network is used with the same skip connections mechanism to bring a solution to cloud removal challenge. Regarding the design of the neural network, DSen2-CR is a fully convolutional network, so it can accept input images of any spatial dimensions (m), as it can be seen in 3. The output of DSen2-CR is a 13-channel layer, representing the thirteen bands from Sentinel2.

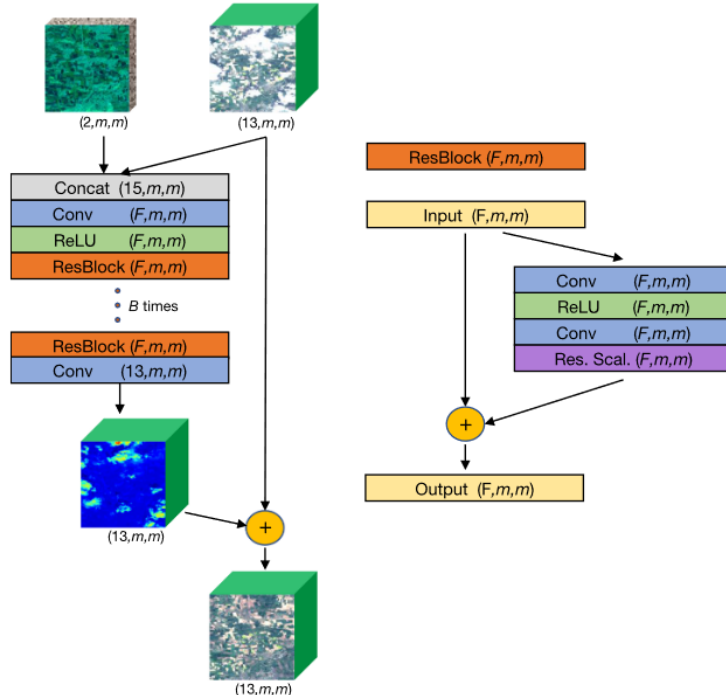


Figure 3: DSen2-CR model diagram.

It also uses Synthetic Aperture Radar (SAR) optical data, which represents an important complementary source to help the model to make greater results. However, SAR images are affected by a particular type of noise called *speckle*, which can difficult network's learning and effectiveness. In addition to that, the model depends on one more source to remove the clouds, as SAR images cannot be downloaded in Sentinel-2. It can be seen in 4 that the lack of SAR data make the network less powerful.

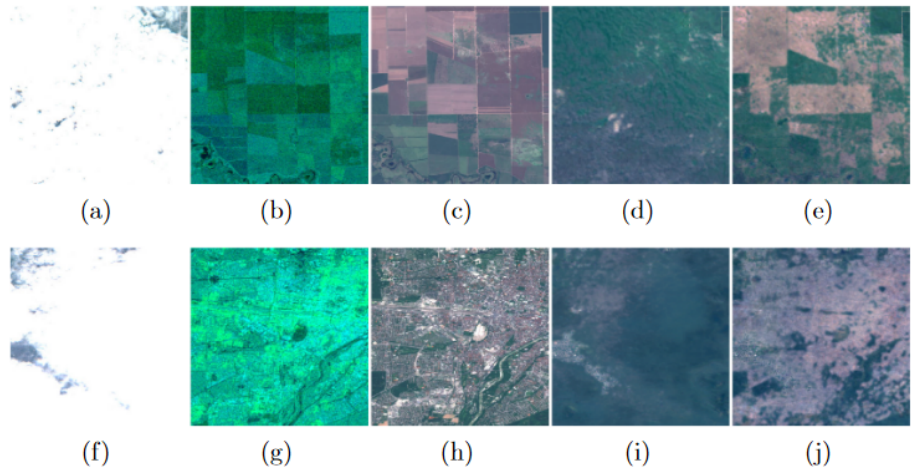


Figure 4: Examples of the influence of SAR data. Being (a, f) cloudy images, (b, g), SAR images, (c, h), the target cloudless images, (d, i), the synthesized images without SAR input data and (e, j) the predictions using SAR data as input.

Improvements have been found using Generative Adversarial Network (GAN) [4], which is a model architecture that belongs to the set of generative models. GAN is an unsupervised model made up of two neural networks: the generator and the discriminator. The idea is based on a game theoretic scenario in which the generator network must compete against an adversary. While the generator network produces samples, the aim of the discriminator is to distinguish between the real samples and the drawn by the generator. The discriminator is a binary classifier trying not to be fooled.

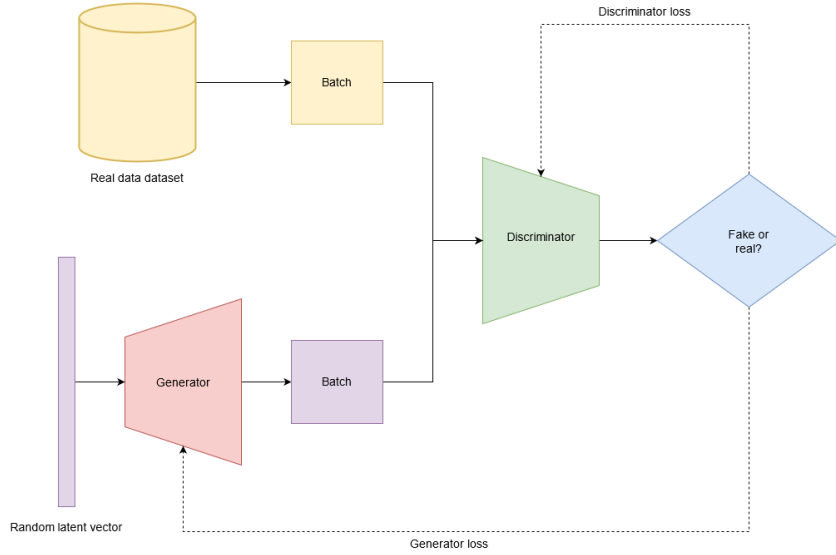


Figure 5: GAN model diagram.

The generator loss is calculated using the discriminator as a reference of how much far is from real images while the discriminator loss is calculated by how much accurate is discerning between the synthesized data and the real one. The standard function can be known as the min-max loss:

$$\begin{aligned} Loss_D(D) &= E_x[\log(D(x))] \\ Loss_G(G) &= E_y[\log(1 - D(G(y)))] \\ Loss_{GAN}(G, D) &= Loss_D(D) + Loss_G(G) \end{aligned}$$

During training, both networks constantly try to outsmart each other, in a zero-sum game. At some point of the training, the game may end up in a state that game theorists call a Nash equilibrium, when no player would be better off changing their own strategy, assuming the other players do not change theirs. GANs can only reach one possible Nash equilibrium: when the generator produces so realistic images that the discriminator is forced to guess by 50 % probability that the image is real or not. Nevertheless, the training process not always can converge to that equilibrium. There are several factors that make the training hard to reach the desired state. For instance, there is a possibility that the discriminator always outsmarts the generator so that it can clearly distinguish between fake and real images. As it never fails, the generator is stuck trying to produce better images as it cannot learn from the errors of the discriminator. Possible solutions can be carried out such as making the discriminator less powerful, decreasing the learning rate or adding noise to the

discriminator target. Another big obstacle is when the generator becomes less diverse, and it learns only to perfectly generate realistic images of a single class, so it forgets about the others. This is called *mode collapse*. At some point, the discriminator can learn how to beat the generator, but then, the latter is forced to do the same but in another class, cycling between classes never becoming good at any of them. A popular technique to avoid is *experience replay*, which consists in storing synthetic images at each iteration in a replay buffer. There is a lot of literature of obstacles and solutions to improve GAN training and it is still very active, as it is in its applications too. The tuning of hyper-parameters and the design of the model will be a key to pursue the Nash equilibrium. For instance, there is a variant called Conditional Generative Adversarial Network (cGAN). Traditionally, the generative network only produces the image from a random vector as an input, which is also called *latent vector* since it cannot be manipulated or with prior convictions of how will be. Unfortunately, this only allows to generate a random image from the domain of the latent space, which is hard to map to the generated images. However, cGAN can be trained so that both generator and discriminator models can be conditioned to some class labels or multi-dimensional vectors and produce synthetic images from a specific domain. In 6, it can be seen a cGAN diagram where the generator is conditioned by some inputs as well as the real data have the condition vector in each sample.

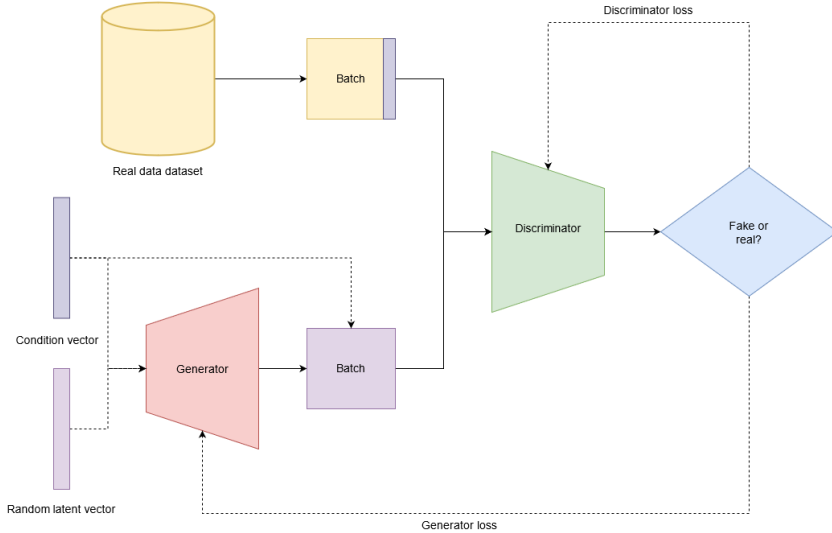


Figure 6: cGAN model diagram.

Actually, it is hard to find another GAN that can fit better in cloud removal problem without being cGAN, since the model needs to be conditioned to the input image. In [5], they proposed a McGAN trained using RGB and NIR cloud-free bands as input and

synthetic RBG cloudy images as target. It is true that short wave bands are unaffected by cloud cover and using NIR images to guide to uncover the clouds of satellite imagery is great since NIR bands posses have higher penetration through fog than visible light bands. Nevertheless, synthesizing the target might not be realistic enough to feasibly deploy the model in real-state. Regarding the experimental results, they have only showed qualitative metrics by comparing the ground-truth with cloud-free images, ones synthesized and ones real, accompanied both by the cloud obscure image and the cloud mask. As the NIR channel is not altered by the perlin noise, there is a huge difference about the effectiveness comparing the synthesized images with the real ones, as it can be seen in 7 and 8

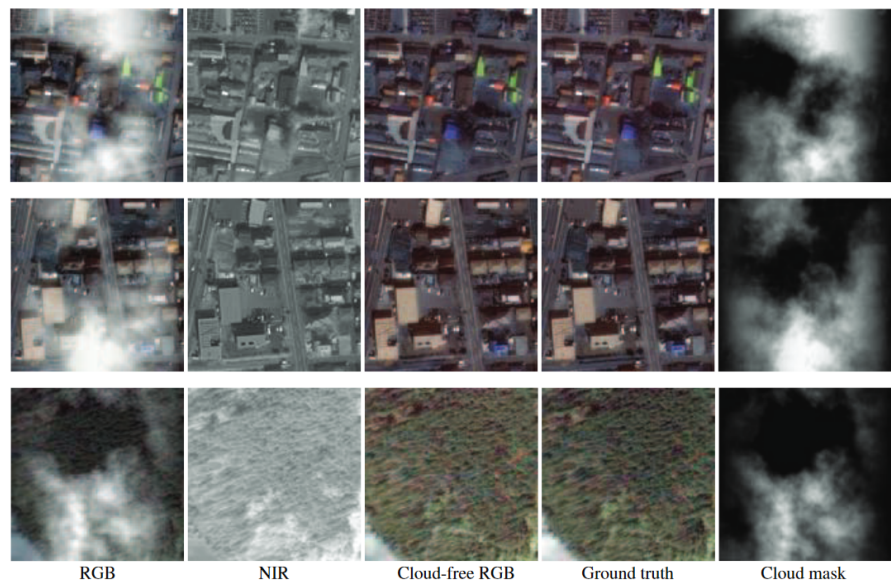


Figure 7: Prediction results by McGAN with the synthesized cloud images

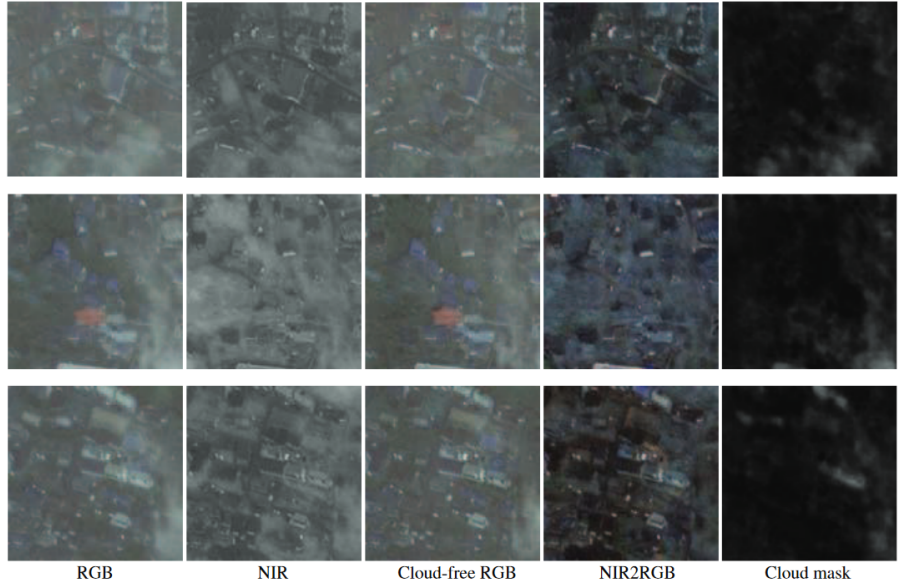


Figure 8: Prediction results by McGAN with the real cloud images

To overcome the need of synthesized data, [6] proposed two datasets and two models respective to each of the datasets. Both neural networks have versions depending on including or excluding the NIR channel as an input. The first is based on Pix2Pix [7] model, a cGAN which performs very well in image-to-image translation tasks. The generator network of Pix2Pix uses a encoder-decoder architecture but with skip-connections to avoid loss of information of the bottleneck, similar to U-Net architecture [8]. The model is trained by a paired dataset of single-images. That means the dataset have a cloudy image as input and a real cloud-free image of the same zone. The generator tries to produce the image as real as the target ones, so it is compulsory to have both images. The second model proposed is a spatio-temporal cGAN trained by pairing clear images with three cloudy corresponding from diverse points in time. Instead of only trying the U-Net architecture as in the first model, they have proposed two designs for the generator:

- A branched ResNet generator. It has three encoder-decoder residual networks to learn feature maps from each image, then concatenating their output to learn from these features again and finally, concatenating the result through a final encoder-decoder to generate the new image.
- A branched U-Net generator. A slightly modification of the U-Net to allow multiple input images to encode them separately but decoding together and skip connections.

Moreover, they have also created two paired datasets to train the single-image models and

the multi-temporal models respectively to overcome the need of synthesizing the images to make them cloud obscured.

Regarding experimental results, they have compared the single-image model with McGAN. On the other hand, they have compared the multi-temporal model with their different versions since it was the first of its kind. The results can be found in 9 and 10. All models from the same comparison were trained using the same datasets created by them. In both cases they have used Peak signal-to-noise ratio (PSNR) and Structural Similarity Index Metric (SSIM) as quantitative metrics and random figure comparison as qualitative metrics. While PSNR is a pixel-based metric capturing the difference between the corresponding pixels from two images, SSIM tracks similarity between visible structures and large-scale features in the images.

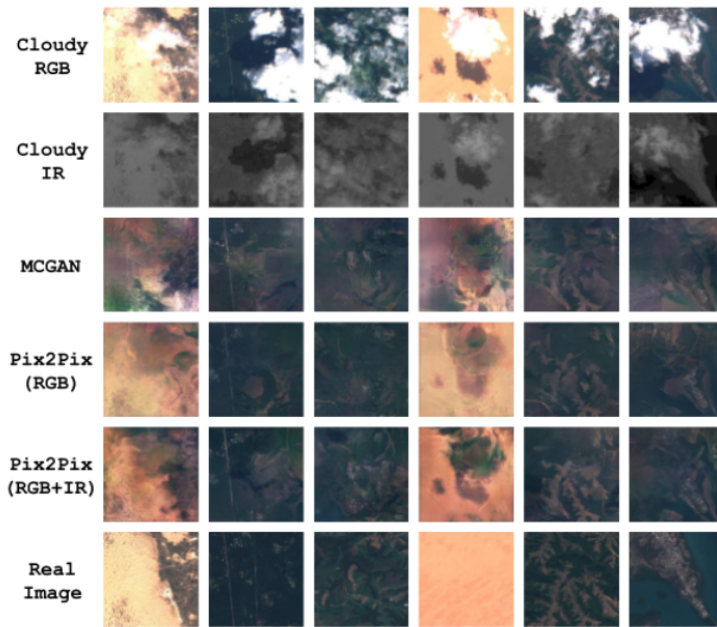


Figure 9: Comparison between the cloudy images, the outputs of McGAN and Pix2Pix-based models and the ground-truth image.

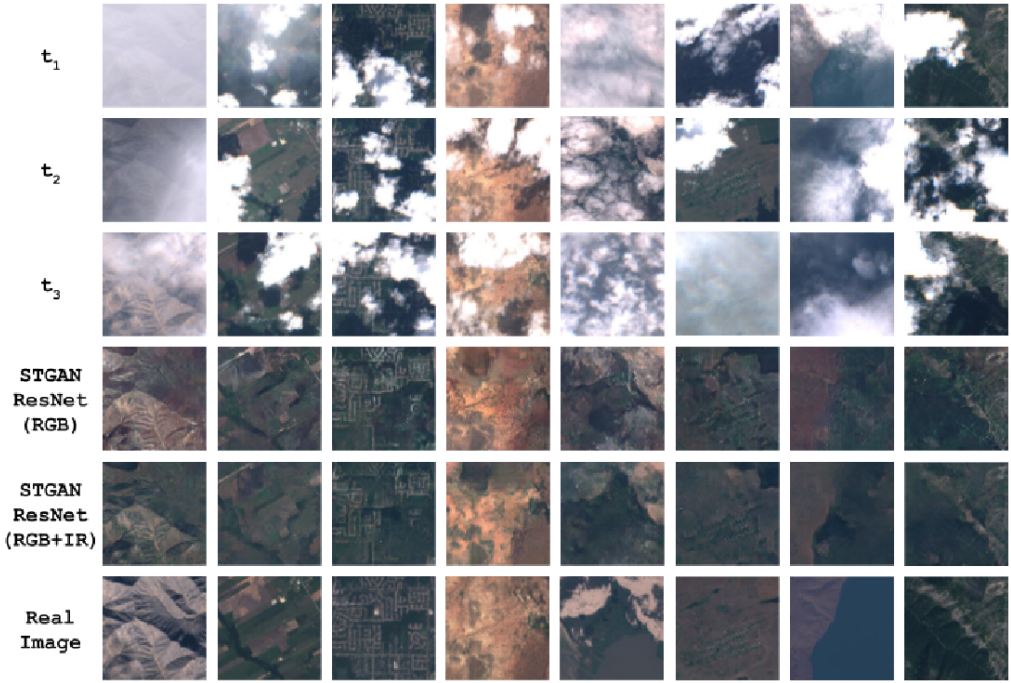


Figure 10: Comparison between cloudy images, the outputs of McGAN versions and the ground-truth image.

Table 2: PSNR and SSIM of the single-image and multi-temporal model versions .

Model	Validation Set		Test Set	
	PSNR	SSIM	PSNR	SSIM
Pix2Pix (RGB)	23.130	0.442	22.894	0.437
Pix2Pix (RGB + IR)	21.352	0.485	21.146	0.481
MCGAN (RGB + IR)	20.871	0.424	21.013	0.381
STGAN U-Net (RGB)	25.484	0.534	25.822	0.564
STGAN ResNet (RGB)	25.519	0.550	26.000	0.573
STGAN U-Net (RGB + IR)	25.142	0.651	25.388	0.661
STGAN ResNet (RGB + IR)	25.628	0.724	26.186	0.734
Raw Cloudy Images	7.926	0.389	8.289	0.422

To overcome the paired-data, Cloud-GAN [9] is a CycleGAN [10] which uses two generators (G_A and G_B) and two discriminators (D_A and D_B). CycleGANs can create new samples of output data, but also transforming the desired data to samples of input data. In essence, they learn to transform data from the two sources by the two generators

respectively being also these sources the target. In other words, CycleGAN is a model that learns two data transformation functions between two domains. In our case, the generator G_A is generating cloud-free images from cloudy images while the generator G_B is turning the cloud-free images into cloudy. Hence, there is no need to train the model by paired cloudy-cloud-free imagery. The datasets for G_A and G_B are respectively:

$$X_A : \{x \mid x \text{ is a real cloud obscured image}\}$$

$$X_B : \{x \mid x \text{ is a real cloud-free image}\}$$

$$X = X_A \cup X_B$$

The synthesized data Y can be split into:

$$Y_A : \{y \mid y \text{ is a synthesized cloud obscured image}\}$$

$$Y_B : \{y \mid y \text{ is a synthesized cloud-free image}\}$$

$$Y = Y_A \cup Y_B$$

$$X_A \cap Y_A = \emptyset, \quad X_B \cap Y_B = \emptyset$$

The transformation functions from each generator can be expressed as:

$$G_A : \text{Generates } y \in Y_B \text{ from } z \in Z_A, \quad Z_A = X_A \cup Y_A$$

$$G_A : Z_A \longrightarrow Y_B$$

$$G_B : \text{Generates } y \in Y_A \text{ from } z \in Z_B, \quad Z_B = X_B \cup Y_B$$

$$G_B : Z_B \longrightarrow Y_A$$

It is well-known that each generator will learn its corresponding transformation function by minimizing the loss, which is calculated by how much the discriminator can discern between their produced data and the real data. On the other hand, the discriminator loss is how good it is to distinguish between the real and the synthesized data.

However, training a cyclic GAN using only the two network losses does not guarantee that cycle consistency is held. Cycle consistency means that given an input, it is desired the back-and-forth transformation $G_B(G_A(z_A)) = z'_A$ to output the the original input z_A . In other words, we want the composition of the transformation functions to be the identity

function.

$$G_A \circ G_B = Id \iff G_B \circ G_A = Id$$

Thus, an additional cycle consistency loss is used to enforce this property. This loss is defined as the uniform norm between an input value z_A from the dataset Z_A and it's forward-cycle prediction $G_B(G_A(z_A))$ and the same for the data $z_B \in Z_B$, $G_A(G_B(z_B))$. The higher the difference, the more distant the predictions are from the original inputs. Ideally, our network would also minimize this loss by a weighting factor λ which is used to control the relevancy of this loss compared to the others.

$$Loss_{Cycle} = E[G_B(G_A(z_A)) - z_A] + E[G_A(G_B(z_B)) - z_B]$$

$$Loss_{CycleGAN} = Loss_{GAN}(G_A, D_A) + Loss_{GAN}(G_B, D_B) + \lambda \cdot Loss_{Cycle}$$

As mentioned before, in [9] they did novel deep learning model for cloud removal, since CloudGAN did not need paired-data and they had promising results removing thin clouds, small cloud patches and synthetic clouds. They have great PSNR in 11 although they could only do it for synthetic clouds as the data is not paired, so that there is no quantitative results for real data, neither a comparison with other models proposed. In addition to that, the images to train and test seem to be not diverse enough since they only download satellite images over Paris region.

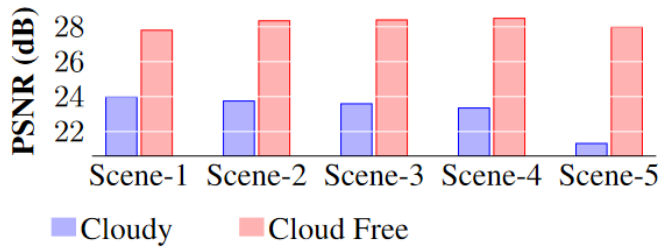


Figure 11: Failure cases in CloudGAN attempting to remove overly clouded images over-smoothing or completely failing.

Even though cyclic GANs work excellently to transforming images to different styles, they seemed to be not enough to create new shapes or providing geometric changes as well as they are not general enough providing unexpected results when the input data fed is quite different from the trained. This issue can be also found in Cloud-GAN as its removal cannot be performed well in overly clouded images 12.

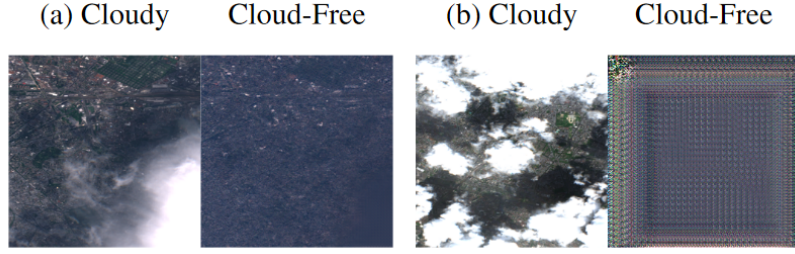


Figure 12: Failure cases in CloudGAN attempting to removal overly clouded images over-smoothening or completely failing.

CNN have worked very well for cloud removal, but latest and disruptive state-of-the-art deep learning attention-based architectures [11] uncover new paths to achieve remarkable improvements and results. It has been demonstrated that transformers can excellently overcome challenges such Natural Language Processing (NLP) [12], Text-To-Image Generation [13] or Image Completion [14] with large datasets, great model size and enough compute.

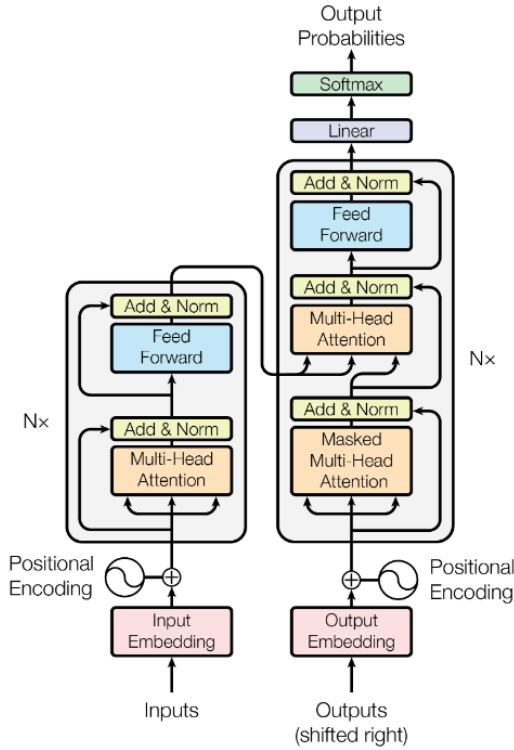


Figure 13: Transformer block architecture.
left block, the encoder architecture, **right block**, the decoder architecture.

The transformer neural network is composed by an encoder-decoder architecture much like Recurrent Neural Network (RNN). However, the difference is that the input sequence

can be passed in parallel by passing also the positional encoder zipped with, as the input might have different meaning depending on its position. Therefore, the positional encoder is a vector that gives context based on position of the element in a sentence. [11] uses a sine and cosine function to generate this vector but it could be any reasonable function.

The input and the positional encoding is passed into the encoder block. The encoder block has N identical encoder layers. Each layer has two sub-layers: a multi-head attention layer and a feed forward layer. Both sub-layers have a residual connection and a layer normalization¹ next to their output vector. When the attention is computed, it means that it is computing what part of the sentence should the network focus. The attention is computed by how relevant is the i^{th} element of the sentence to other words in the same sentence. Therefore, we can understand the attention as a vector that captures the contextual relationships between elements in the sentence. The feed-forward layer is a network that is applied to every one of the attention vectors. This layer is used to turn these vectors into a form that the next encoder or decoder block can get as an input.

Regarding the decoder block, it has several similarities with the encoder block. They both have N identical layers and a position encoding. However, the decoder layer have a masked multi-head attention layer before the multi-head attetion layer and the feed forward layer. This is because the encoder can use all the elements of the input sentence but the decoder can only use the previous elements $\{ j^{\text{th}} \text{ element } | j < i \}$ of the sentence. By not doing that, there would be no learning at all. The output of the decoder block is passed into a linear layer, which is an another feed forward layer. Finally, the output is passed to a softmax layer to have a better understanding of the output data as it returns a probability distribution.

¹The normalization is done by each feature instead by each sample.

2.3 Academic Datasets

3 Model architecture

4 Experiments & results

5 Conclusions

6 Bibliography

References

- [1] Charis Lanaras, José Bioucas-Dias, Silvano Galliani, Emmanuel Baltsavias, and Konrad Schindler. Super-resolution of sentinel-2 images: Learning a globally applicable deep neural network. *ISPRS Journal of Photogrammetry and Remote Sensing*, 146:305–319, 2018.
- [2] Kaiming He, Xiangyu Zhang, Shaoqing Ren, and Jian Sun. Deep residual learning for image recognition. In *Proceedings of the IEEE conference on computer vision and pattern recognition*, pages 770–778, 2016.
- [3] Andrea Meraner, Patrick Ebel, Xiao Xiang Zhu, and Michael Schmitt. Cloud removal in sentinel-2 imagery using a deep residual neural network and sar-optical data fusion. *ISPRS Journal of Photogrammetry and Remote Sensing*, 166:333 – 346, 2020.
- [4] Ian Goodfellow, Jean Pouget-Abadie, Mehdi Mirza, Bing Xu, David Warde-Farley, Sherjil Ozair, Aaron Courville, and Yoshua Bengio. Generative adversarial nets. In *Advances in neural information processing systems*, pages 2672–2680, 2014.
- [5] Kenji Enomoto, Ken Sakurada, Weimin Wang, Hiroshi Fukui, Masashi Matsuoka, Ryosuke Nakamura, and Nobuo Kawaguchi. Filmy cloud removal on satellite imagery with multispectral conditional generative adversarial nets. In *2017 IEEE Conference on Computer Vision and Pattern Recognition Workshops (CVPRW)*, pages 1533–1541, 2017.
- [6] Vishnu Sarukkai, Anirudh Jain, Burak Uzkent, and Stefano Ermon. Cloud removal in satellite images using spatiotemporal generative networks. *arXiv preprint arXiv:1912.06838*, 2019.

- [7] Phillip Isola, Jun-Yan Zhu, Tinghui Zhou, and Alexei A Efros. Image-to-image translation with conditional adversarial networks. *CVPR*, 2017.
- [8] Olaf Ronneberger, Philipp Fischer, and Thomas Brox. U-net: Convolutional networks for biomedical image segmentation, 2015. cite arxiv:1505.04597Comment: conditionally accepted at MICCAI 2015.
- [9] Praveer Singh and Nikos Komodakis. Cloud-gan: Cloud removal for sentinel-2 imagery using a cyclic consistent generative adversarial networks. In *IGARSS 2018 - 2018 IEEE International Geoscience and Remote Sensing Symposium*, pages 1772–1775, 2018.
- [10] Jun-Yan Zhu, Taesung Park, Phillip Isola, and Alexei A Efros. Unpaired image-to-image translation using cycle-consistent adversarial networks. In *Computer Vision (ICCV), 2017 IEEE International Conference on*, 2017.
- [11] Ashish Vaswani, Noam Shazeer, Niki Parmar, Jakob Uszkoreit, Llion Jones, Aidan N. Gomez, Łukasz Kaiser, and Illia Polosukhin. Attention is all you need. In Isabelle Guyon, Ulrike von Luxburg, Samy Bengio, Hanna M. Wallach, Rob Fergus, S. V. N. Vishwanathan, and Roman Garnett, editors, *Advances in Neural Information Processing Systems 30: Annual Conference on Neural Information Processing Systems 2017, 4-9 December 2017, Long Beach, CA, USA*, pages 6000–6010, 2017.
- [12] Tom B. Brown, Benjamin Mann, Nick Ryder, Melanie Subbiah, Jared Kaplan, Prafulla Dhariwal, Arvind Neelakantan, Pranav Shyam, Girish Sastry, Amanda Askell, Sandhini Agarwal, Ariel Herbert-Voss, Gretchen Krueger, Tom Henighan, Rewon Child, Aditya Ramesh, Daniel M. Ziegler, Jeffrey Wu, Clemens Winter, Christopher Hesse, Mark Chen, Eric Sigler, Mateusz Litwin, Scott Gray, Benjamin Chess, Jack Clark, Christopher Berner, Sam McCandlish, Alec Radford, Ilya Sutskever, and Dario Amodei. Language models are few-shot learners, 2020. cite arxiv:2005.14165Comment: 40+32 pages.
- [13] Aditya Ramesh, Mikhail Pavlov, Gabriel Goh, Scott Gray, Chelsea Voss, Alec Radford, Mark Chen, and Ilya Sutskever. Zero-shot text-to-image generation. In Marina Meila and Tong Zhang, editors, *Proceedings of the 38th International Conference on Machine Learning*, volume 139 of *Proceedings of Machine Learning Research*, pages 8821–8831. PMLR, 18–24 Jul 2021.

- [14] Mark Chen, Alec Radford, Rewon Child, Jeffrey Wu, Heewoo Jun, David Luan, and Ilya Sutskever. Generative pretraining from pixels. In Hal Daumé III and Aarti Singh, editors, *Proceedings of the 37th International Conference on Machine Learning*, volume 119 of *Proceedings of Machine Learning Research*, pages 1691–1703. PMLR, 13–18 Jul 2020.